Organically modified vanadium pentoxide as cathode for aqueous zinc ion batteries

Yanyao Han

A thesis
submitted in partial fulfillment of the
requirements for the degree of

Master of Science

University of Washington
2023

Committee:
Guozhong Cao
Lucien N. Brush

Program Authorized to Offer Degree:
Materials Science & Engineering

University of Washington

Abstract

Organically modified vanadium pentoxide as
cathode for aqueous zinc ion batteries

Yanyao Han

Chair of the Supervisory Committee:
Guozhong Cao
Department of Materials Science & Engineering

Aqueous zinc ion batteries (ZIBs) have attracted a lot of attention due to its environment-friendly, safe, easy to assemble, low-cost, and high capacity. Among the various ZIBs cathode materials, vanadium-based oxides have shown great potential for inexpensive, highly safe, spacious ion transport channels and excellent electrochemical performance. Despite these promises, the development of aqueous ZIBs is still hindered by irreversible formation of by-products, low electronic conductivity, sluggish Zn-ion diffusion, and poor structural stability. This study developed a high performance pre-inserted acetone hydrated vanadium pentoxide (AVOH) by modifying the vanadium pentoxide structure through hydrothermal process. As a result, the obtained Zn/AVOH batteries possess a higher capacity of 428 mA h g^{-1} at 50 mA g^{-1} and an impressive rate capability with 60 % capacity maintained when the current density increased from 0.5 to 8.0 A g^{-1}, showing promising application as aqueous ZIBs.

TABLE OF CONTENTS

1. Introduction

With the increasing energy demand and environmental concern, the development of renewable and clean energy resources has attracted significant attention [1-3]. To date, lithium-ion batteries (LIBs), benefiting from high gravimetric energy density, long cycle life, and lightweight, have been broadly used in electric vehicles and smart electronics as mature technology. However, there are some concerns about LIBs that impede the development for multi-purpose energy storage, such as the safety issue, high cost and deficiency of lithium assets in the earth [4-6]. Besides of new process to improve the safety of LIBs and reduce cost, developing alternative rechargeable batteries, such as lithium-sulfur batteries, other alkali metal-ion (Na^+ and K^+) batteries, and multivalent ion (Zn^{2+}, Mg^{2+}, Ca^{2+}, and Al^{3+}) batteries has become a major concern [7]. Sodium-ion batteries (SIBs) and potassium-ion batteries (PIBs) have gained a lot of attention in recent years because the rich resources and low cost, while the use of organic electrolytes in batteries continues to pose a safety issue [8, 9]. Given these circumstances, the foremost concern should be the safety of the batteries, as well as ensuring the necessary electrochemical performance and cost-effectiveness. Aqueous zinc-ion batteries (ZIBs) are currently considered to be promising candidates because of the following advantages: low cost due to its natural abundance [10, 11]; high volumetric energy density (5851 mA h cm^{-3}) [12]; high stability and ionic conductivity in aqueous electrolytes [13]; multiple electron transfer during electrochemical reactions enable high energy and high-power density [14]. Furthermore, the assembly of aqueous ZIBs does not need to be performed in a glove box, which greatly simplifies the manufacturing process [15].

The first ZIBs was invented by Volta in 1799 which relied on the excellent properties of zinc as an anode material. After that, various other batteries were created, including Zn-Mn [16], Zn-Ag [17], Ni-Zn [18], and Zn-air [19, 20]. In the 1970s, a rechargeable Zn-MnO_2 battery was made available for consumer use [21]. The energy storage mechanism in this type of alkaline Zn-MnO_2 battery was a conversion reaction, but the cathode and anode were prone to irreversible side reactions, leading to a short cycle life, low performance stability, and an instability to charge and discharge at high current [22]. Despite these limitations, this application played a significant role in the development of alkaline batteries. In 1986, Yamamoto et al. first replaced the alkaline electrolyte with zinc sulfate electrolyte and tested the performance of the resultant battery [23]. In recent years, aqueous ZIBs have gained popularity due to their various benefits such as environment-friendly, safe, easy to assemble, low-cost, and high capacity. However, the lack of cost-effective cathode materials with high storage capacities and structural stability is the major obstacle to the grid-scale application of ZIBs [24]. Substantial efforts have been made to find the most appropriate cathode materials for aqueous ZIBs. To date, these are the materials exploited as cathode materials for aqueous ZIBs, including manganese-based compounds, vanadium-based materials, Prussian blue and its analogous, and organic redox-active compounds. The most frequently used type of cathode materials for ZIBs, the problem they encountered and feasible solutions will be discussed comprehensively in the next section. This article will also state a route to modify vanadium pentoxide as the cathode for aqueous ZIBs, which can improve electrochemical activity and stability in the long term. The paper concludes by suggesting some potential directions for future research on cathode materials and examines the prospects of aqueous ZIBs.

Table 1. Comparison of the partial parameters among Zn and other metal cations as charge carriers for batteries [13,15]

Element	Li	Na	Zn	Mg	Al	Ca	K
Ionic Radius(Å)	0.76	1.02	0.74	0.72	0.54	1.00	1.38
Standard Potential (V vs. SHE)	-3.04	-2.71	-0.76	-2.36	-1.67	-2.86	-2.92
Proportion/%	0.0017	2.36	0.0075	2.9	8.2	5	2.09
Theoretical Gravimetric Capacity (mA h g^{-1})	3862	1166	820	2205	2980	1340	686
Theoretical Volumetric Capacity (mA h cm^{-3})	2062	1128	5851	3833	8046	2073	610
Cost($/lb)	8-11	1.1-1.6	0.5-1.5	1-1.5	0.5-1.5	-	3-9

2. Cathode materials

The cathode materials used in ZIBs have a major influence on the energy and power density of the battery. The performance of the cathode, including ionic and electronic transport properties and redox reaction kinetics, significantly affects the rate performance and gravimetric power density. The stability and integrity of the cathode structure are equally important as the anode in determining the cycling stability of a battery system. Researchers have faced significant challenges in developing cathode materials with high storage capacity, high discharge potential, and a robust crystal structure that allows for easy insertion and extraction of zinc ions. Currently, only a few materials, such as manganese-based compounds, vanadium-based materials, Prussian blue and its analogs, and organic redox-active compounds, have been used as feasible Zn-ion host materials. This section provides a summary of the various cathode materials that have been discussed for use in aqueous ZIBs. It covers the different types of materials, the issues they face, and possible solutions.

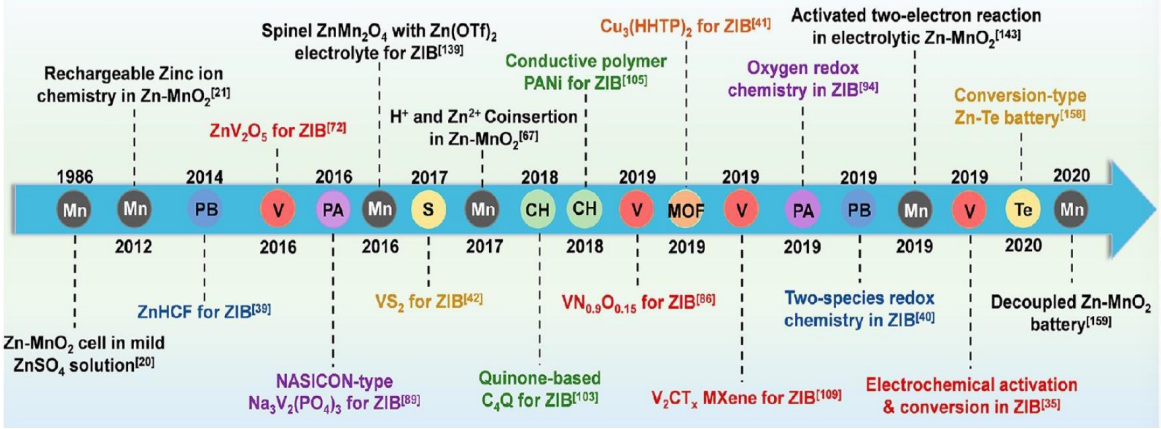

Figure 1. Main progress and brief development history of cathode materials. Reproduced with permission from [25].

2.1 Manganese-based materials

Due to the advantages of safety, affordability, rich source, eco-friendliness, and manganese-based oxides with various states (Mn^{2+}, Mn^{3+}, Mn^{4+} and Mn^{7+}), manganese-based oxides are supported to be very promising cathode materials for aqueous ZIBs [26, 27].The most widely used manganese-oxides in aqueous ZIBs is MnO_2, one of the reasons is it has the most abundant crystal structures (as shown in **Fig. 2**), including α-MnO_2, β-MnO_2, λ-MnO_2, todorokite MnO_2, δ-MnO_2, R-MnO_2 and so on [28]. Up to now, numerous research has been done about different crystal structure's MnO_2 as cathode material for aqueous ZIBs. The results show that the different crystal structure can lead to the differences in electrochemical performance. Unlike more established systems such as lithium-ion batteries and sodium-ion batteries, the energy storage mechanism of aqueous ZIBs is more complex and has not been fully explained yet. Up to date, there are four storage mechanisms proposed, including Zn^{2+} insertion/extraction, reversible Zn^{2+} and H^+ co-insertion/extraction, chemical conversion reaction, and dissolution/deposition [29].

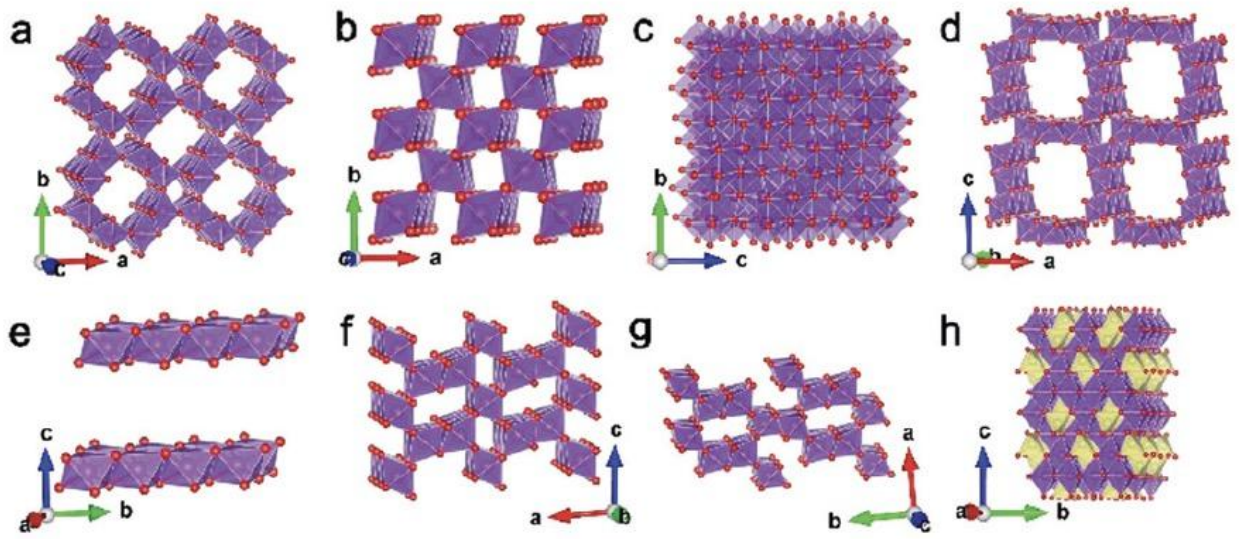

Figure 2. Schematic diagram of various crystal structures of manganese-based materials: (a) α-MnO_2; (b) β-MnO_2; (c) λ- MnO_2; (d) todorokite MnO_2; (e) δ- MnO_2; (f) γ- MnO_2; (g) R- MnO_2; (h) $ZnMn_2O_4$. Reproduced with permission from [30]. Copyright 2019 Energy Environment Science.

Although MnO_2 is a promising cathode material for aqueous ZIBs due to its safety, high voltage output, high capacity, and environmental kind, its practical application and growth is hindered by three major issues: (1) Instability in structure. During the repetitive charge/discharge process, all manganese oxides suffer from structural damage and volume change leading to serious capacity fading. (2) Manganese ion dissolution. The active material dissolves into the electrolyte which can result in rapid capacity attenuation. (3) Poor electrical conductivity. The sluggish electrons transport kinetics can limit the electrons transfer rate [29].

2.2 Vanadium-based materials

Vanadium-based materials are widely used in LIBs and SIBs due to its abundant resources, low cost, and high theoretical capacity [31, 32]. In addition, the multiple valence states (V^{2+}, V^{3+}, V^{4+}, V^{5+}) and versatile V-O polyhedron structure leads to different crystal structure and diverse composition (**Fig. 3**). To date, several vanadium-based structures have demonstrated to serve as

cathode for aqueous ZIBs, including VxOy, metal vanadate, and vanadium phosphates. In the following section, we mainly focus on V_2O_5 and discuss the problem it faces, and some strategies researchers tried.

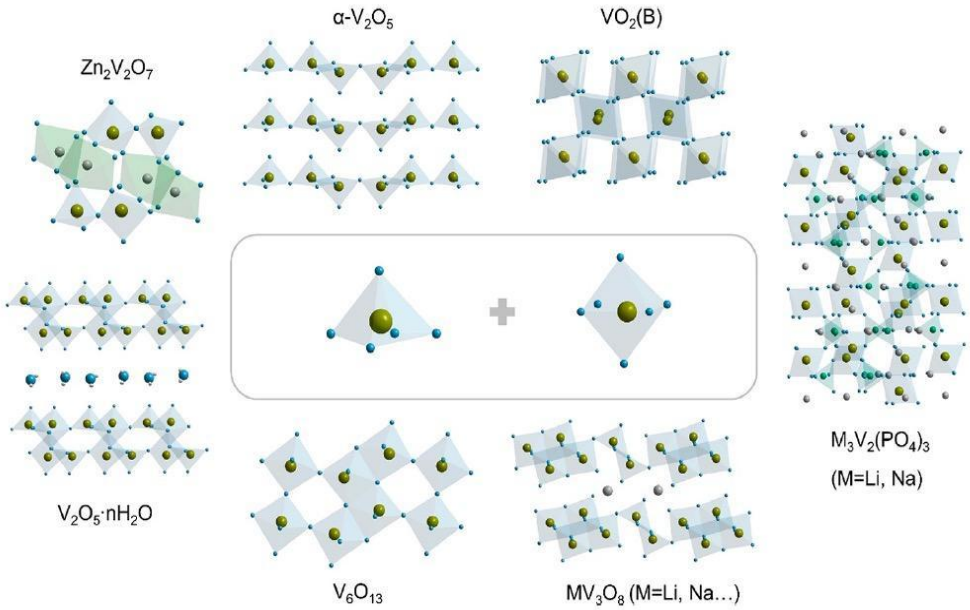

Figure 3. Typical crystal structure of vanadium oxides. Reproduced with permission from [14]. Copyright 2020 Chemical Reviews.

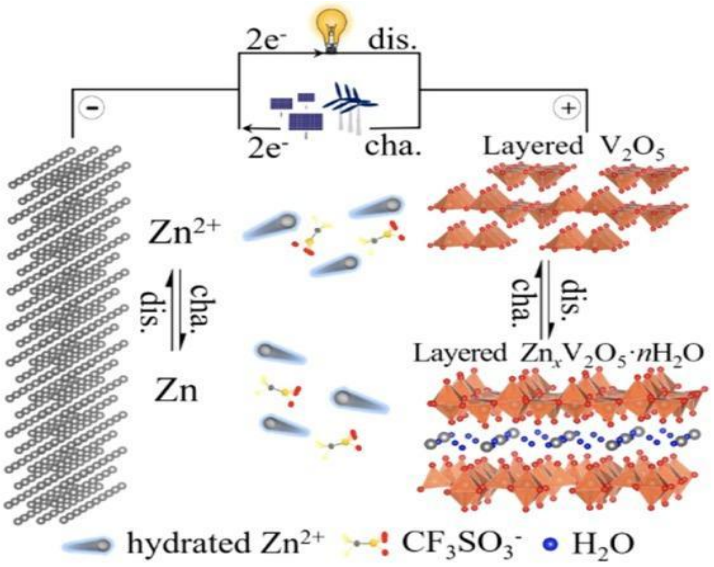

Figure 4. Schematic illustration of the rechargeable aqueous Zn−V_2O_5 battery chemistry. Reproduced with permission from [33]. Copyright 2018 ACS Energy Letters.

V_2O_5 is a promising cathode material for aqueous ZIBs due to low cost, high theoretical capacity (589 mA h g^{-1}), and great potential [33]. V_2O_5 has a layered structure which is formed by stacking VO_5 square pyramids in either an edge-sharing or corner-sharing arrangement [34]. The unique layered structure makes Zn^{2+} easily insert/extract between the interlayer due to the weaker Van der Waals force and hydrogen bonds between the layers [35]. The storage mechanism of V_2O_5 as cathode for aqueous ZIBs is simple, upon discharging, Zn^{2+} ion and water molecular co-intercalate into the layered V_2O_5 structure, and the phase transform from V_2O_5 to a new layered phase $Zn_xV_2O_5 \bullet nH_2O$. And during the charge process, the layered phase will revert to V_2O_5 (**Fig. 4**). However, there are some critical problems that need to be solved. During the repetitive charge/discharge process, the layered structure of V_2O_5 will suffer from structure deterioration which leads to the serious capacity decay. For example, the initial discharge capacity of porous V_2O_5 as cathode material in $Zn(CF_3SO_3)_2$ electrolyte is 201mAh g^{-1} at a rate of 100mA g^{-1}, however, the capacity decreases to 73mAh g^{-1} after 90 cycles [36]. Another problem is the low interlayer spacing which causes low capacity. Upon discharging, the strong attraction between Zn^{2+} and H_2O results in Zn binding six H_2O in its solvation shell, $[Zn(H_2O)_6]^{2+}$, increasing the size of a bare Zn^{2+} from 0.74Å to 5.5Å. The large molecule $[Zn(H_2O)_6]^{2+}$ is hard to be intercalated into most electroactive materials. Discovering the material that has high interlayer spacing to allow $[Zn(H_2O)_6]^{2+}$ to be directly intercalated with structural stability and high electrical conductivity has attracted increasing attention.

Some researchers discovered that hydrated vanadium pentoxide ($V_2O_5 \bullet nH_2O$) is more promising than V_2O_5 as the cathode for metal ion batteries. Liu et al. developed $V_2O_5 \bullet nH_2O$/graphene (VOG) material through liquid phase method [37]. VOG exhibits high capacity (381 mA h g^{-1}) when current density is 60 mA g^{-1} and long cycling stability (71% maximum

capacity retention after 900 cycles at 6 A g^{-1}). The water molecule between the V_2O_5 interlayer plays the function of reducing the electrostatic interaction between Zn^{2+} and V_2O_5 framework by shielding the effective charge of Zn^{2+}. In addition, the structural water also can enlarge V_2O_5 interlayer spacing to 12.6 Å which allows Zn^{2+} insertion/de-insertion smoothly. Due to these benefits of adding structural molecules, high capacity and stability has been achieved.

To further enhance the electrochemical performance, researchers found that mixed vanadium valence cathode can increase the electrical conductivity via electron hopping between V^{4+} and V^{5+} [38]. Liang et al first used VOOH as the precursor to synthesize V^{4+}-V_2O_5 with mixed vanadium valances. Compared with V_2O_5 without V^{4+}, V^{4+}-V_2O_5 shows high capacity and excellent stability (140 mA h g^{-1} after 1000 cycles at 10 A g^{-1}) due to its faster ion diffusion capability, lower polarization, and higher electrical conductivity. Furthermore, Kim et al. synthesized two-dimensional V_2O_5 nanoflakes by self-doped V^{4+} ions from ammonium vanadate [39]. The formed V_2O_5 nanoflakes consist of large amounts of V^{4+} ions, which can prompt higher electrical conductivity, high capacity (430 mA h g^{-1} at 0.5 A g^{-1}) and excellent reversibility (86% capacity retention after 1000 cycles).

To expand the interlayer spacing to accommodate hydrated Zn^{2+} insertion, some metal ions such as Mg^{2+}, Cu^{2+}, Ca^{2+}, K^{+}, Na^{+}, Li^{+}, Mn^{2+}, Co^{2+} have been used to pre-intercalate into the V_2O_5 interlayers [25]. Liu et al. synthesized manganese expanded hydrated vanadate (MnVO) through one step hydrothermal process [40]. MnVO cathode shows significantly high specific capacity (415 mA h g^{-1} at a current density of 50 mA g^{-1}) and excellent stability (92% capacity retention over 2000 cycles). The insertion of Mn^{2+} expands the interlayer spacing to 12.9 Å compared to

11.9 Å of VOH without Mn^{2+} pre-insertion. The expanded interlayer facilitates ionic transportation and high electronic conductivity. The appearance of V^{4+} by introducing of Mn^{2+} can further expand the lattice spacing due to larger ionic radius and enhance the electrical conductivity. The chemical bond between Mn^{2+} and [VO_n] layers can stabilize the structure and thus guarantees excellent structural stability and high-capacity retention upon repetitive cycling. The comparison of metal ion stabilized V_2O_5 materials suggests that the interlayer spacing is determined by the hydrated radius not the ionic radius. Despite the smaller hydrated Li^+ ions than other hydrated divalent ions, Li^+ pre-intercalated V_2O_5 shows the largest interlayer spacing. This result shows that the interlayer space might also be affected by the charge of the pre-intercalated ions.

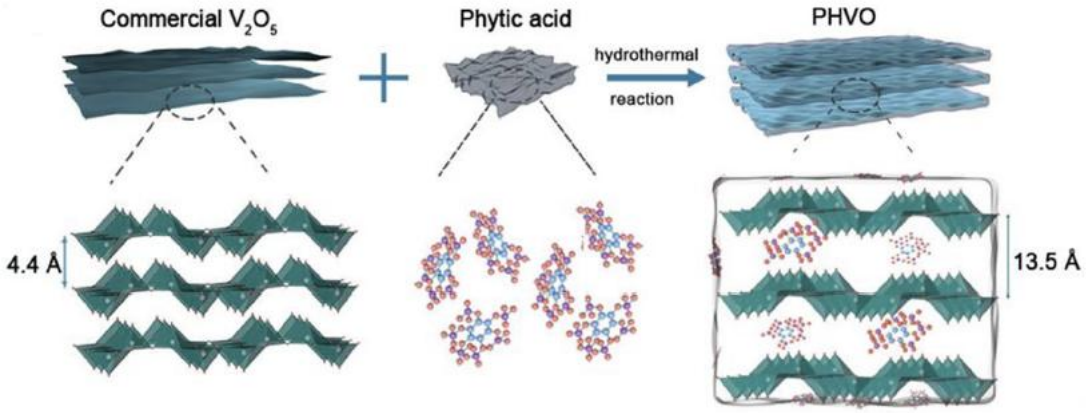

Figure 5. Schematic illustration for the synthetic route of phytic acid coated/inserted-V_2O_5 (PHVO) and structure of commercial V_2O_5, phytic acid and PHVO. Reproduced with permission from [41]. Copyright 2022 Applied Surface Science.

In addition to metal cations, the organic material can also be the guest species to stabilize the V_2O_5 structure. For example, the synthesis of phytic acid coated/inserted V_2O_5 (PVOH) can be obtained by one-step hydrothermal method [41]. The obtained PVOH cathode shows excellent

specific capacity (406 mA h g^{-1} at 0.1 A g^{-1}), and high stability (97.3% capacity retention after 6000 cycles at 5A g^{-1}). The superior electrochemical performance of PVOH can ascribed to the following reasons. First, the phytic acid formed a uniformly ultrathin layer coated on the V_2O_5 surface to stabilize the crystal structure during the long cycling process. Second, the existence of phytic acid expands the V_2O_5 interlayer distance to 13.5 Å, facilitates the diffusion kinetics of Zn^{2+} and therefore contributes to better rate capability [41].

2.3 Prussian blue and its analogues

Prussian blue analogs (PBAs) can act as ZIBs cathode materials due to it has multiple number of interstitial sites which can act as storage sites for Zn^{2+}. The general formula for a PBAs system is typically represented as $A_xM_1[M_2(CN)6]_y \bullet nH_2O$, where A is usually an alkali metal atoms such as Li, Na, or K, and M_1 and M_2 are transition metal atoms such as Mn, Co, Ni, Fe, Cu, or Zn [14]. The original Prussian blue, $Fe_4^{III}[Fe^{II}(CN)_6]3 \bullet nH_2O$ has a face centered cubic structure where M_1^{II} and Fe^{III} are situated alternatively on the corners of smaller cubes and connected by C≡N bonds; the low-spin Fe^{III} forms bonds with only C atoms while the high-spin M^{II} forms bonds with N atoms (**Fig. 6**). The C/N bonds create openings in the faces of the elementary cubes which allow for metal ions to move between the half-filled body center positions [42].

PBAs can provide numerous benefits for secondary energy storage: (1) The 3D diffusion channels within the electrode materials can improve ion transport; (2) The synthesis methods for PBAs are straightforward, inexpensive, and prone to large-scale application; (3) PBAs can have uncreased capacity through double electron redox reaction design. Although the above benefits and PBAs offer the highest potential operating voltage (around 1.7 vs Zn^{2+}/Zn), the use as Zn^{2+}

intercalation cathodes have been greatly hindered by low specific capacity (around 80mA h g^{-1}), poor performance during repeated cycles, and low Coulombic efficiency.

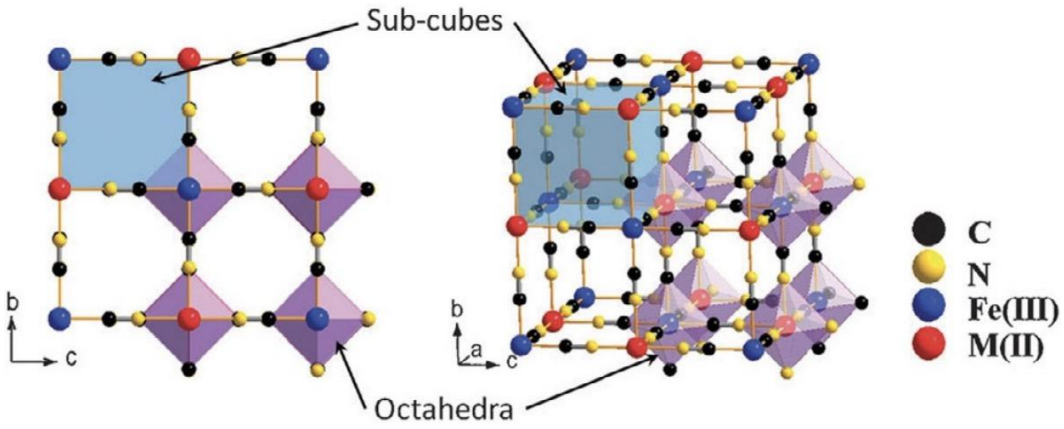

Figure 6. The framework of Prussian blue analogs. Reproduced with permission from [42]. 2020 Chemistry-A European Journal.

2.4 Organic Materials

Organic compound materials can be promising ZIBs cathode due to the following reasons: (1) The composition of organic materials only includes low-cost and environmental-friendly elements such as C, H, O, N, S. This means that organic materials do not include heavy metals and can be synthesized indefinitely without depleting resources; (2) The adjustable structure of organic materials enables them to modify the structure of organic molecules to reach desired the electrochemical properties; (3) The redox reaction that occurs during the charging and discharging of organic cathode materials is limited to the chemical absorption and ions doping, without changing the organic structure. This results in a highly structure stability during the charge and discharge process; (4) The organic cathode material is suitable for use in univalent (Li^+, Na^+, K^+, H^+), divalent (Zn^{2+}, Mg^{2+}, Ca^{2+}), and even multivalent such as Al^{3+} metal ion batteries [43].

Organic electrode materials are categorized into p-type, n-type, and bipolar types based on the changes in the free radical state of the active site. The reaction mechanism of n-type organic materials is similar to inorganic materials. The redox center can be reduced to produce anions and create sites for zinc ion insertion. In contrast, the p-type organic materials transfer electrons from the conjugated main chain, leaving positive charges on the chain and reach the electric neutrality through the electrolyte during charging. Bipolar type materials can be reduced or oxidized within a specific voltage range and their charging process is like that of p-type organics. The change in valence of bipolar type materials is accompanied by the insertion and removal of anions. Although the multiple advantages of organic materials, such as the fast reaction kinetics, and adjustable structure, the development of high-performance as cathode is still a challenge. The main reason is the dissolution of discharged products in electrolytes result to poor cycle life.

3. Experiment

3.1 Synthesis of materials

All the chemicals were used as received without further purification. 2 mmol of V_2O_5 (99.6+%, Sigma-Aldrich) and 2 mL of H_2O_2 (30 %, Fisher Chemical) were successively added into 50 mL of deionized (DI) water under constant stirring for 20 minutes. The different volumes of C_3H_6O (0.1mL, 0.15mL, 0.25mL, 0.5mL) was dissolved into 30 mL of DI water to yield a homogeneous solution. Mixed the two solutions and transferred to a 100 mL Teflon lined stainless steel autoclave and heated to 120 ℃ and kept at this temperature for 6 h. The product was collected and dried in a freeze dryer at -52 ℃ for 3 - 4 days. Based on the volume of acetone that added in the reaction solution (0.1mL, 0.15mL, 0.25mL, 0.5mL), the obtained materials were denoted as AHVO-0.1, AHVO-0.15, AVOH-0.25, AVOH-0.5). The hydrated vanadium pentoxide (VOH)

was synthesized with the same procedure with AVOH without adding C_3H_6O in the reaction solution.

3.2 Characterization of materials

The prepared samples were characterized by Bruker X-ray diffractometer (D8 Discover with IμS 2-D detection system) with an accelerating voltage of 50 kV and a working current of 1000 μA. A differential scanning calorimeter (DSC 3+ STAR^e System, Mettler Toledo) was adopted to analyze the thermal stability of the sample within 40–700 ℃ in flowing nitrogen gas (50 sccm). The surface chemical states of the materials were detected using a Kratos Axis-Ultra DLD X-ray photoelectron spectroscopy system (XPS) with a monochromatized AlKα X-ray and a low energy electron flood gun for charge neutralization. The angle between the sample normal and the input axis of the energy analyzer was 0°.

3.3 Electrochemical tests

The cathode was prepared by mixing active material, conductive carbon and polyvinylidene fluoride (PVDF) in a weight ratio of 7: 2 : 1 using N-methyl-2-pyrrolidone (NMP) as solvent to obtain a slurry that was pasted on a current collector - titanium foil. The electrodes with mass loading of active materials at 3 - 4 mg cm^{-2} were further dried in a vacuum oven at 120 ℃ for 12 h. The electrochemical properties were tested using CR2032 type cells with Zn metal as the anode and 3M zinc trifluoromethanesulfonate (98%, $Zn(CF_3SO_3)_2$) aqueous solution as electrolyte. A glass fiber filter (Whatman, Grade GF/A) was used as the separator.

The cathode materials' redox properties were tested by cyclic voltammetry on a Solartron electrochemical station at a scan rate of 0.1 to 1.2 mV s^{-1}. The Galvanostatic charge and discharge tests were conducted using a Neware tester at room temperature. The reaction resistance in the electrochemical process was analyzed using a galvanostatic intermittent titration technique, performed at a current density of 50 mA g^{-1} with charging and discharging time and 10 min interval for each step. The electrochemical impedance spectroscopy (EIS) measurements were performed on the Solartron electrochemical station from the frequency range of 0.01 Hz to 10^5. The working voltage of the cells was set from 0.2 to 1.6 V versus Zn^{2+}/Zn.

4. Results and discussion

4.1 Materials characterization

Fig. 7 shows XRD patterns of hydrated vanadium pentoxide (VOH) without acetone insertion and different amount acetone added AVOH. The XRD pattern of VOH is accurately matched with the standard peaks of $V_2O_5 \bullet nH_2O$ (PDF 40-1296). It is hypothesized that AVOH's structure involves stacked V-O double layers, and the adjacent layers are separated by water and acetone added in the preparation. Compared with VOH, the (0 0 1) crystal plane peak of AVOH-0.15, AVOH-0.25, AVOH-0.5 all have shifted to a lower angle. This can be explained by the insertion of acetone can lead to the shift of (0 0 1) Bragg reflections. But it should note that the interplanar spacing of AVOH-0.1 is the same with AVOH due to the amount of acetone pre-inserted is too small to increase the interlayer spacing. **Table 2** shows the (0 0 1) peak position and interlayer space of VOH and AVOH. The interlayer spacing increase as the added amount of acetone increase which means the interlayer distances are positively associated with the content of acetone.

To confirm the effects of acetone on the structural stability, DSC/TGA is used to analyze the water loss in the heating process. From **Fig. 8**, it is worth noting that the water content in AVOH-0.5 (12.6 %) is less than that in VOH (13.7 %).

Table 2. The calculated interlayer distance based on (0 0 1) peak.

Sample ID	2-Theta (°)	d-Spacing (Å)
VOH	7.54	11.71
AVOH-0.1	7.54	11.71
AVOH-0.15	7.50	11.77
AVOH-0.25	7.48	11.80
AVOH-0.5	6.58	13.42

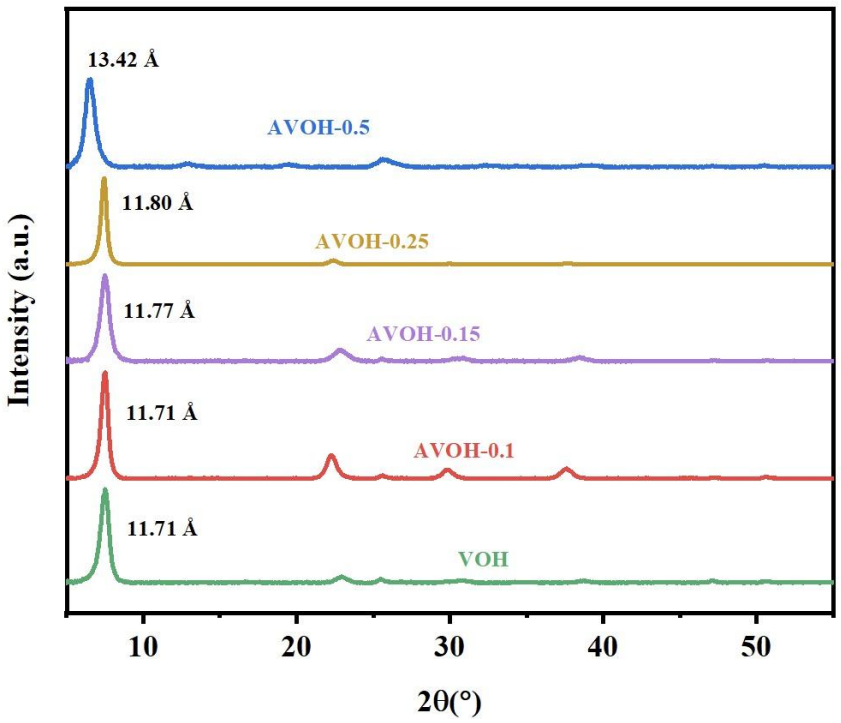

Figure 7. XRD pattern of AVOH and VOH

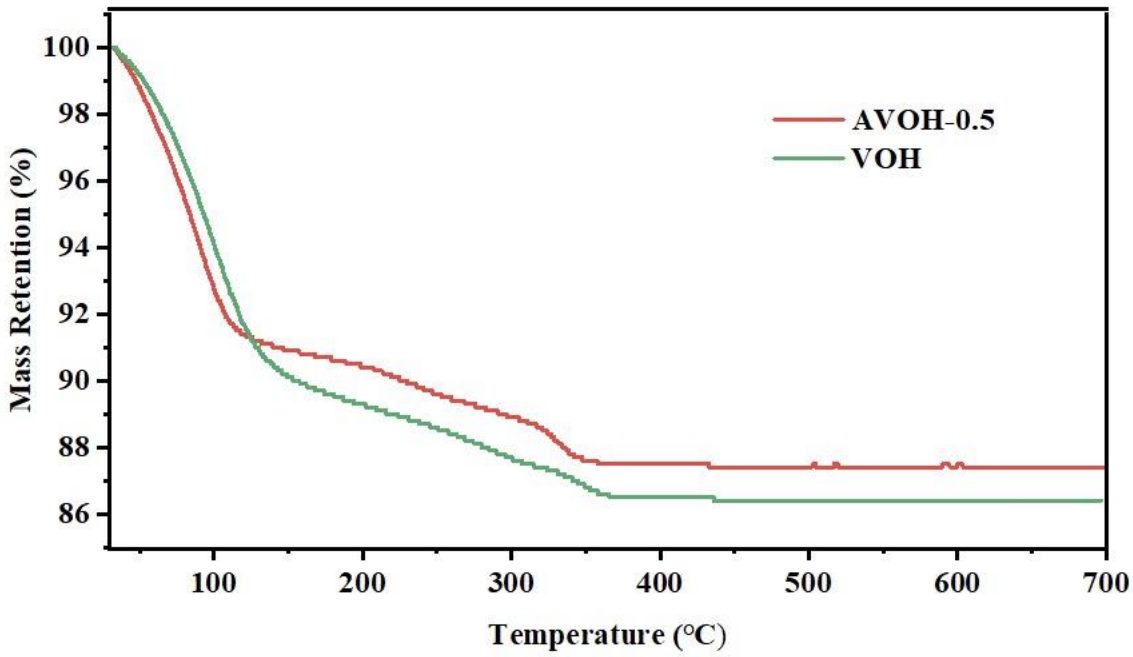

Figure 8. TGA/DSC curves of AVOH-0.5 and VOH within 30-700 ℃

The X-ray photoelectron spectroscopy (XPS) of AVOH-0.1 shown as **Fig 9a.** has the similar spectra peak with VOH which means they have the similar elemental composition. The V $2p_{3/2}$ spectra show mixed V^{5+} and V^{4+} valance states in AVOH-0.1 (**Fig. 9b**). The higher binding energy of 517.4 eV observed at the peak center was attributed to the presence of V^{5+} oxidation state, whereas the lower binding energy of 516.2 eV was assigned to V^{4+}. The appearance of V^{4+} in AVOH-0.1 is possibly from a reduction reaction between V_2O_5 and H_2O_2 to form $VO(O_2)$ in the synthesis process. The existence of V^{4+} implies the appearance of oxygen vacancies which can serve as catalyst for the electrochemical process of aqueous ZIBs. The lattice spacing further expands due to V^{4+} has a bigger ionic radius of 72 pm compared to that of 68 pm for V^{5+} in six coordination. From the high-resolution results of carbon (**Fig 9c.**), the binding energy of 287.06 eV shows the existence of carbonyl. The area ratio of C-C/C-H: C-C=O is 8 : 1 which

corresponds to the structure of acetone. These results confirms that acetone has successfully inserted into the V_2O_5 interlayer spacing.

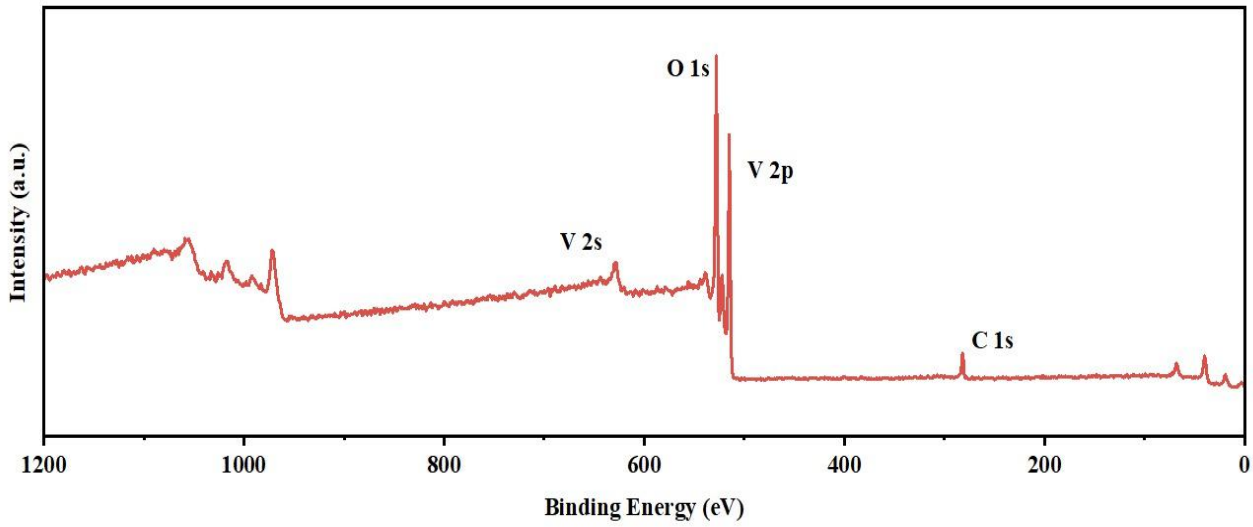

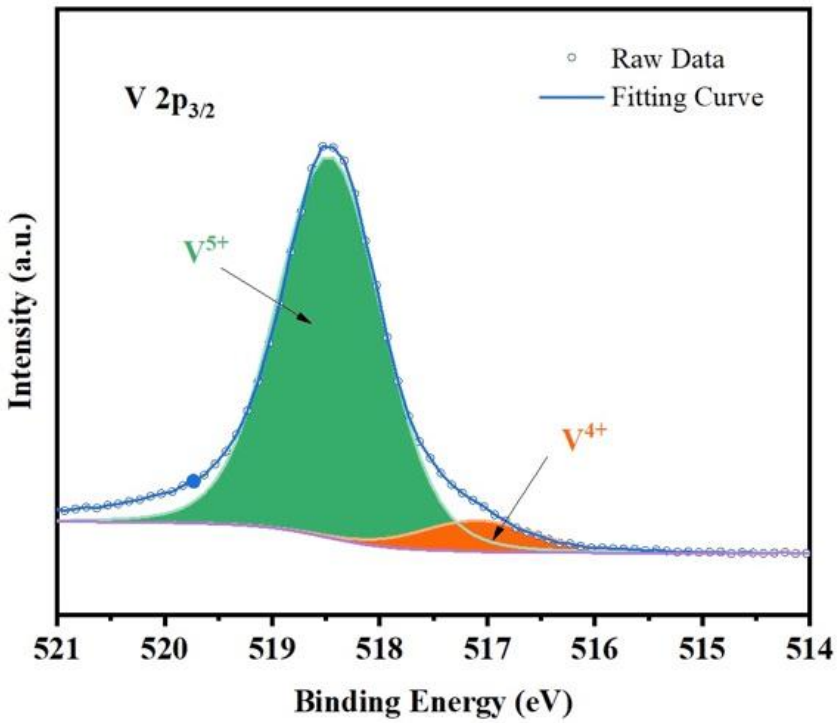

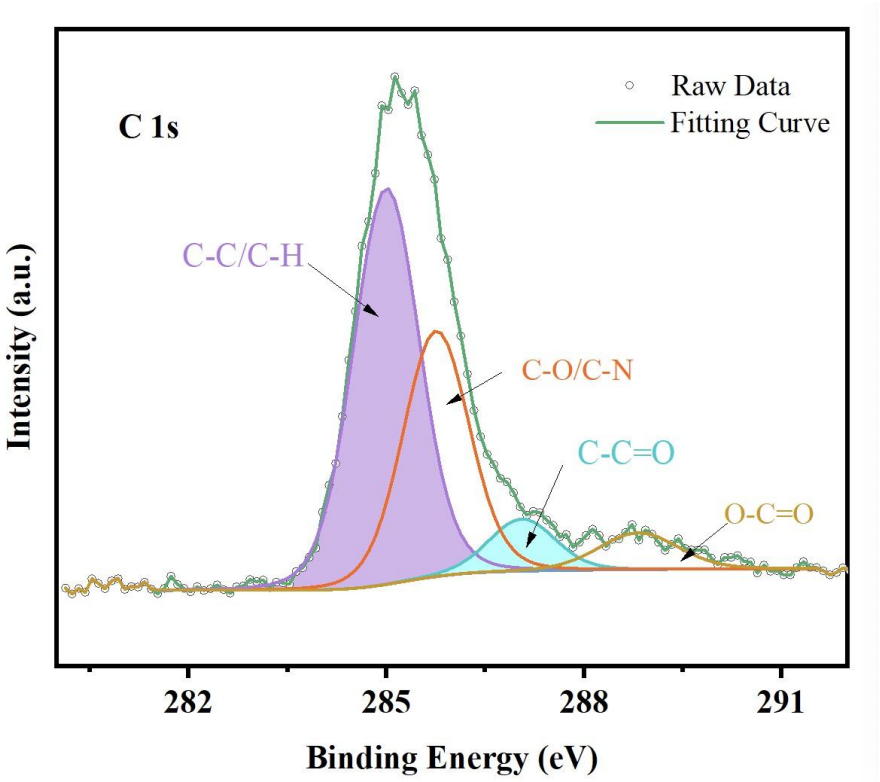

Figure 9. (a) the XPS results of AVOH-0.1 (b) high-resolution results of Vanadium (c) high-resolution results of Carbon.

4.2 Electrochemical behavior

Fig. 10a displays the first three cyclic voltammetry (CV) curves of Zn/AVOH-0.1 cells tested within the voltage range of 0.2-1.6V (vs. Zn^{2+}/Zn) at a scan rate of 0.1mV s^{-1}. Two pairs of redox peaks suggesting multi-steps for the Zn^{2+} insertion. The peaks around ~1.0V and 0.5V are related to the redox reaction of V^{5+}/V^{4+} and V^{4+}/V^{3+} pairs, respectively. The overlapped CV curves in the initial three cycles suggest a highly reversible reaction of the AVOH-0.1 cathode in the aqueous ZIBs. The initial discharge peak around 1 V shifts to a higher voltage in the subsequent cycles which could happen due to modification of local chemical surroundings after zinc ion insertion.

The CV curves for AVOH-0.1 and VOH are compared in **Fig. 10b**, which were obtained at a speed of 0.1 mV s-1. The difference between two samples is that AVOH-0.1 possess a larger current response and a larger integrated area of CV curves in comparison to that of VOH (as summarized in **Table 3**), indicating a larger capacity of AVOH-0.1. Additionally, the smaller voltage difference between each pair of redox peaks in AVOH-0.1 compared to VOH indicates lower polarization and improved reversibility, resulting in better electrochemical kinetics for AVOH-0.1 electrodes.

Table 3. The redox pairs and voltage differences in VOH and AVOH-0.1

Sample ID	Redox pairs (V)	Peak Voltages (V)	Peak separation (V)
VOH	V^{5+}/V^{4+}	0.91/1.02	0.11
	V^{4+}/V^{3+}	0.46/0.61	0.15
AVOH-0.1	V^{5+}/V^{4+}	0.97/1.04	0.08
	V^{4+}/V^{3+}	0.48/0.58	0.10

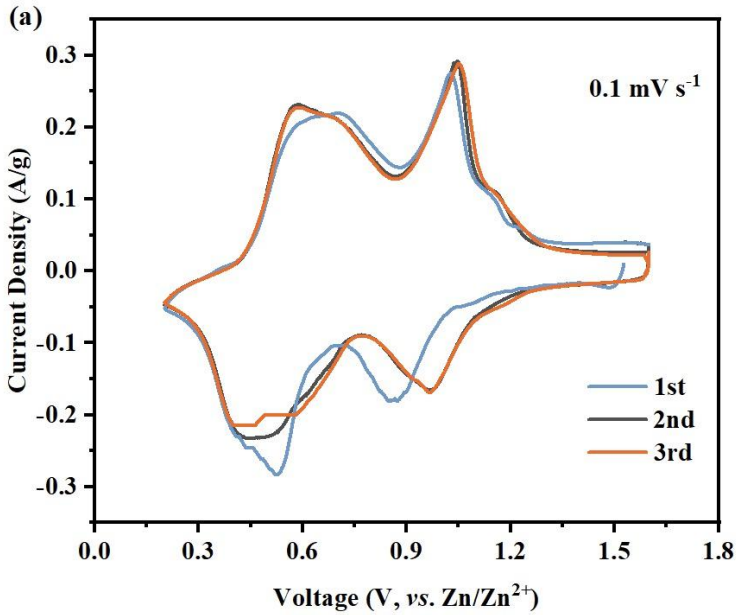

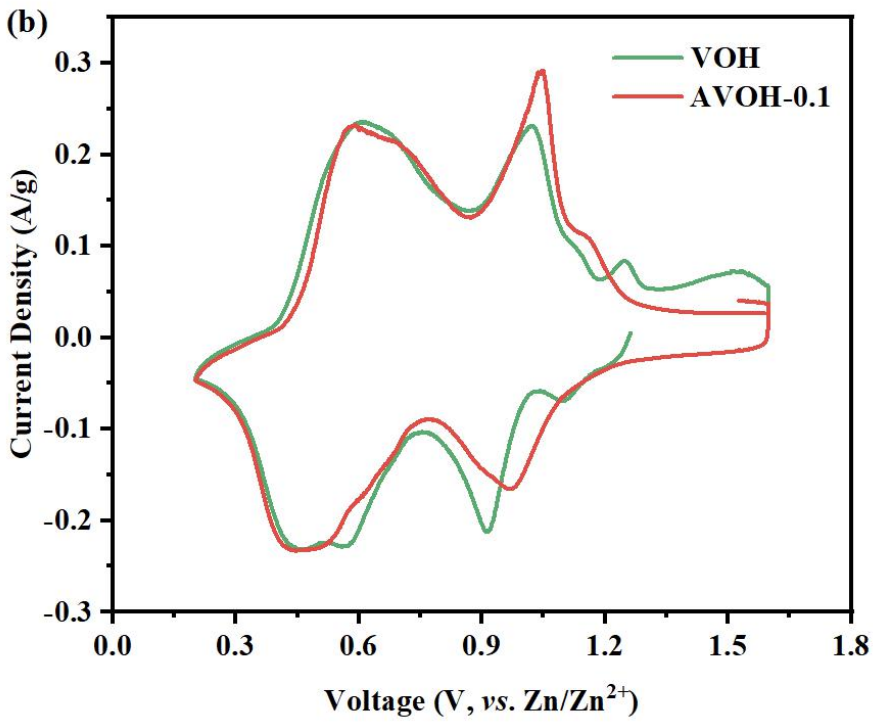

Figure 10. (a) CV curves of AVOH-0.1 collected at a sweep rate of 0.1 mV s^{-1}. The overlapping of the curves in the first three cycles means good reaction reversibility in AVOH-0.1. (b) Comparison of the CV curves of VOH and AVOH-0.1. The similar shape indicates the same redox reaction in VOH and AVOH-0.1.

Fig. 11a shows the galvanostatic discharge (Zn^{2+} insertion) and charge (Zn^{2+} de-insertion) (GCD) curve of the first three cycles for AVOH at a current density of 50 mA g^{-1}. The two pairs of charge/discharge plateaus match the two pairs of redox peaks seen in the CV curves (**Fig. 10a**). AVOH-0.1 has specific capacity of 428 mA h g^{-1} which is higher than that of other vanadium-based cathodes, such as $Na_2V_6O_{16}$ nH_2O, LiV_3O_8 or $H_2V_3O_8$. And the well overlapped GCD curve indicates the repetitive charge/discharge process is highly reversible.

The GCD profiles of the samples are displayed in **Fig. 11b**. At a current density of 50 mA g^{-1}, AVOH-0.1 has a discharge capacity of 428 mA g^{-1}, which is greater than VOH's capacity of 360

mA g^{-1}. AVOH-0.1 also has a smaller voltage gap between its charge and discharge profiles compared to VOH. This suggests that AVOH-0.1 has highly reactive reversibility and reduced polarization.

Rate responses of AVOH-0.1 and VOH are compared in **Fig. 11c**. The discharge capabilities of AVOH-0.1 at 0.5, 1.0, 2.0, 4.0, and 8.0 A g^{-1} are 358, 330, 300, 260, and 207 mA h g^{-1}, respectively, and VOH exhibits capacities of 336, 314, 284, 240, and 176 mA h g^{-1} at the corresponding conditions. Even when the current density increases to 8.0 A g^{-1}, AVOH-0.1 still has a high reversibility of 207 mA h g^{-1}. The capacity retention in AVOH-0.1 is 58%, which is higher than that of 51% in VOH, at 8 A g^{-1}, compared with their capacities at 0.5 A g^{-1}. When the rate returns to 0.5 A g^{-1}, the capacity recovers to the initial values, indicating a stable crystal structure and the high electrochemical reversibility of AVOH-0.1.

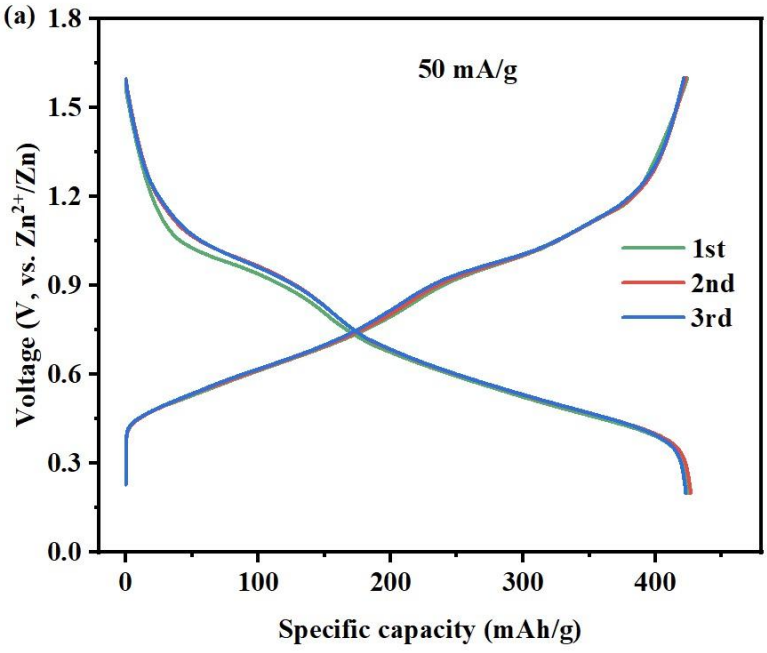

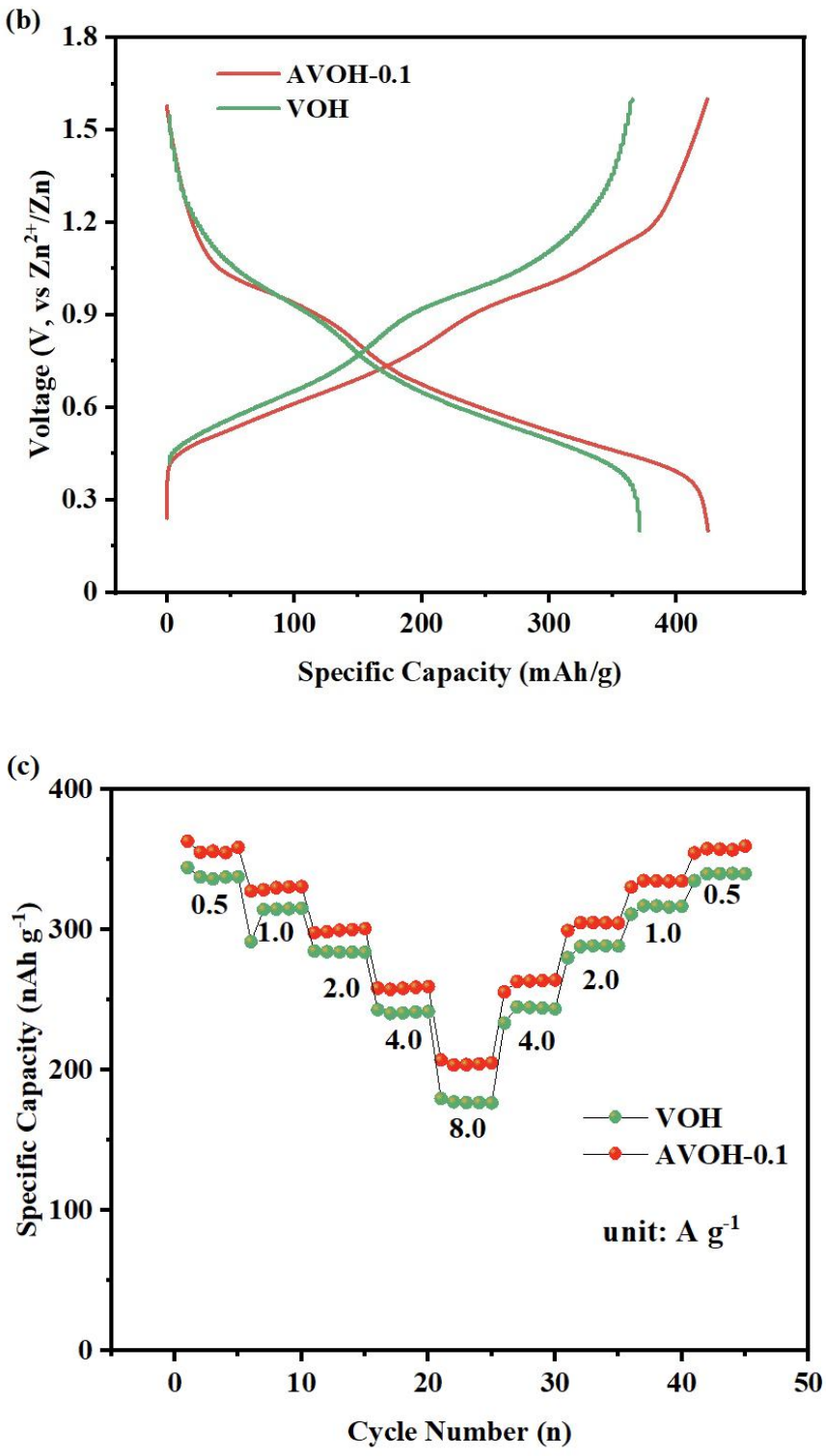

Figure 11. (a) First three cycles voltage profiles of AVOH-0.1 at 50 mA g-1. (b) GCD profiles and (c) Rate capability of AVOH-0.1 and VOH.

5. Conclusion and future work

In conclusion, we added different amount of acetone through the one-step hydrothermal process to get new cathode material for aqueous ZIBs. By adding 0.1 mL acetone, the crystal structure of VO_x can be stabilized upon cycling. Pre-inserted acetone hydrated vanadate (AVOH-0.1) has the same redox reaction with VOH during the charge/discharge process. AVOH-0.1 possess a larger storage capacity (428 mA h g^{-1}) at 50 mA g^{-1} compared to that of VOH (360 mA h g^{-1}) and an impressive rate capability with 58 % capacity maintained when the current density increased from 0.5 to 8.0 A g^{-1}, showing promising application as aqueous ZIBs.

Future works mainly focuses on analyzing the Zn^{2+} storage mechanism in AVOH cathode, try different molecular ratios of vanadium pentoxide and acetone, use post-synthesis treatment approach to synthesis AVOH cathode, and design other organic pre-inserted material as ZIBs cathode.

(1) To better understand how Zn^{2+} is stored in the AVOH cathode, it's necessary to analyze the changes in structure and vanadium's valance state during Zn^{2+} intercalation and de-intercalation, as well as the phase transformations that occur during cycling. We can accomplish this by using *ex situ* XRD analysis and *ex situ* X-ray photoelectron spectroscopy analysis at various states of charge and discharge and supplement these analyses with energy-dispersive X-ray spectroscopy to map the distribution of Zn, V and O elements.

(2) Previous thermogravimetric results show one VOH molecule contains 1.6 chemically bonded H_2O molecule. We will try the molecular ratios of acetone and vanadium pentoxide ratios: 0.3, 0.6, 1, and 1.6 for partially and completely replacing the water molecules in hydrated vanadium pentoxides.

(3) Try to insert different kinds of highly polar and large-sized organic molecules into the vanadium pentoxide interlayer as cathode materials.

The cathode materials based on vanadium have several benefits such as being inexpensive, highly safe, having spacious ion transport channels and exhibited excellent electrochemical performance. Despite these promises, the development of aqueous ZIBs is hindered by the lack of high-performance cathodes and complicated energy storage mechanisms. There are several significant challenges to overcome, including the co-intercalation of protons and zinc ions leads to an increase in PH and the formation of by-products, the dissolution of transition metal cations from cathodes causes capacity decay, and the large gaps in redox potentials result in low energy conversion efficiency.

Reference

[1] Larcher, D.; Tarascon, J. M.; Towards Greener and More Sustainable Batteries for Electrical Energy Storage. Nat. Chem. 2015, 7, 19−29.

[2] Kwade, A.; Haselrieder, W.; Leithoff, R.; Modlinger, A.; Dietrich, F.; Droeder, K. Current Status and Challenges for Automotive Battery Production Technologies. *Nat. Energy.* 2018, 3, 290−300.

[3] Li, M.; Lu, J.; Chen, Z.; Amine, K. 30 Years of Lithium-Ion Batteries. Adv. Mater. 2018, 30, 1800561.

(4) Liu, X.; Ren, D.; Hsu, H.; Feng, X.; Xu, G. L.; Zhuang, M.; Gao, H.; Lu, L.; Han, X.; Chu, Z.; et al. Thermal Runaway of Lithium-Ion Batteries without Internal Short Circuit. Joule 2018, 2, 2047−2064.

(5) Liu, B.; Jia, Y.; Li, J.; Yin, S.; Yuan, C.; Hu, Z.; Wang, L.; Li, Y.; Xu, J. Safety issues caused by internal short circuits in lithium-ion batteries. J. Mater. Chem. A 2018, 6, 21475−21484.

(6) Abada, S.; Marlair, G.; Lecocq, A.; Petit, M.; Sauvant-Moynot, V.; Huet, F. Safety focused modeling of lithium-ion batteries: A review. J. Power Sources 2016, 306, 178−192.

[7] Hwang, J.; Myung, S.; Sun Y. Sodium-ion batteries: Present and future, Chem. Soc. Rev. 2017, 46, 3529–3614.

[8] Desai, A.; Morris, R.; Armstrong, A. Advances in organic anode materials for Na-/K-ion rechargeable batteries, ChemSusChem, 2020, 13, 4866–4884.

[9] Ding, G.; Zhu, L.; Yang, Q.; Xie, L.; Cao, X.; Wang, Y.; Liu, J.; Yang, X. NaV3O8/poly (3,4-ethylenedioxythiophene) composites as high-rate and long-lifespan cathode materials for reversible sodium storage, Rare Met. 2020, 39, 865–873.

[10] Zhang, L.; Chen, L.; Zhou, X.; Liu, Z. Towards High-Voltage Aqueous Metal-Ion Batteries Beyond 1.5 V: The Zinc/Zinc Hexacyanoferrate System. Adv. Energy Mater. 2015, 5, 1400930.

[11] Xu, C.; Li, B.; Du, H.; Kang, F. Energetic Zinc Ion Chemistry: The Rechargeable Zinc Ion Battery. Angew. Chem., Int. Ed. 2012, 51, 933−935.

[12) He, P.; Quan, Y. L.; Xu, X.; Yan, M. Y.; Yang, W.; An, Q. Y.; He, L.; Mai, L. Q. High-Performance Aqueous Zinc-Ion Battery Based on Layered H2V3O8 Nanowire Cathode. Small 2017, 13, 1702551.

[13] Massé, R.C.; Uchaker, E.; Cao, G. Beyond Li-ion: electrode materials for sodium- and magnesium-ion batteries. Sci. China Mater. 2015, 58, 715–766.

[14] Jia, X.; Liu, C.; Neale, Z.G.; Yang, J.; Cao, G. Active Materials for Aqueous Zinc Ion Batteries: Synthesis, Crystal Structure, Morphology, and Electrochemistry. Chem Rev. 2020, 120(15), 7795-7866.

[15] Zhou, T.; Zhu, L.; Xie, L.; Han, Q.; Yang, X.; Chen, L.; Wang, G.; Cao, X. Cathode materials for aqueous zinc-ion batteries: A mini review. J Colloid Interface Sci. 2022, 605, 828-850.

[16] Xue, T.; Fan, H.J. From aqueous Zn-ion battery to Zn-MnO_2 flow battery: A brief story, J. Energy Chem. 2021, 54, 194–201.
[17] Liang, G.; Mo, F.; Wang, D.; Li, X.; Huang, Z.; Li, H.; Zhi, C. Commencing mild Ag–Zn batteries with long-term stability and ultra-flat voltage platform, Energy Storage Mater. 2020, 25, 86–92.
[18] Zhu, X.; Wu, Y.; Lu, Y.; Sun, Y.; Wu, Q.; Pang, Y.; Shen, Z.; Chen, H. Aluminumdoping-based method for the improvement of the cycle life of cobalt-nickel hydroxides for nickel-zinc batteries, J. Colloid Interface Sci. 2021, 587, 693–702.
[19] Gu, P.; Zheng, M.; Zhao, Q.; Xiao, X.; Xue, H.; Pang, H. Rechargeable zinc–air batteries: A promising way to green energy, J. Mater. Chem. A 2017, 5, 7651–7666.
[20] Armand, M.; Tarascon, J.-M. Building better batteries, Nature 2008, 451, 652–657.
[21 Gabano, J.P.; Morignat, B.; Laurent, J.F. 4-variation of physico-chemical parameters in an alkaline MnO_2-Zn cell during discharge, Power Sources: Research and development in non-mechanical electrical power sources 4, 1967, 49–63.
[22] Yang, J.; Cao, J.; Peng, Y.; Yang, W.; Barg, S.; Liu, Z.; Kinloch, I.; Bissett, M.; Dryfe, R.A.W. Unravelling the mechanism of rechargeable aqueous Zn-MnO_2 batteries: Implementation of charging process by electrodeposition of MnO_2, ChemSusChem, 2020, 13, 4103–4110.
[23] Tang, B.; Shan, L.; Liang, S.; Zhou, J. Issues and opportunities facing aqueous zinc-ion batteries, Energy Environ. Sci. 2019, 12, 3288–3304.
[24] Zhang, T.; Tang, Y.; Guo, S.; Cao, X.; Pan, A.; Fang, G.; Zhou, J.; Liang, S. Fundamentals and perspectives in developing zinc-ion battery electrolytes: a comprehensive review. Energy and Environmental Science, 2020, 13, 4625-4665.
[25] Wang, X.; Zhang, Z.; Xi, B.; Chen, W.; Jia, Y.; Feng, J.; Xiong, S. Advances and Perspectives of Cathode Storage Chemistry in Aqueous Zinc-Ion Batteries, ACS Nano. 2021, 15, 9244-9272.
[26] Pan, H.; Shao, Y.; Yan, P.; Cheng, Y.; Han, K.; Nie, Z.; Wang, C.; Yang, J.; Li, X.; Bhattacharya, P.; Mueller, K. T.; Liu, J. Reversible Aqueous Zinc/Manganese Oxide Energy Storage from Conversion Reactions. Nat. Energy 2016, 1, 16039.
[27] Zhang, N.; Cheng, F.; Liu, J.; Wang, L.; Long, X.; Liu, X.; Li, F.; Chen, J. Rechargeable Aqueous Zinc-Manganese Dioxide Batteries with High Energy and Power Densities. Nat. Commun. 2017, 8, 405.
[28] Juran, T.R.; Young, J.; Smeu, M. Density functional theory modeling of MnO_2 polymorphs as cathodes for multivalent ion batteries, J. Phys. Chem. C, 2018, 122, 8788–8795.
[29] Xu, Y.; Zhang, G.; Liu, J.; Zhang, J.; Wang, X.; Pu, X.; Wang, J.; Yan, C.; Cao, Y.; Yang, H. Recent advances on challenges and strategies of manganese dioxide cathodes for aqueous zinc-ion batteries. Energy & environmental materials, 2022.

[30] Tang, B.; Shan, L.; Liang, S.; Zhou, J. Issues and opportunities facing aqueous zinc-ion batteries. Energy & environmental science. 2019, 12, 3288–334.
[31] Mohamed, N.; Allam, N.K. Recent advances in the design of cathode materials for Li-ion batteries. RSC Adv. 2020, 10, 21662–21685.
[32] Zhu, L.; Ge, P.; Xie, L.; Miao, Y.; Cao, X. Doped-Li1+xV_3O_8 as cathode materials for lithium-ion batteries: A mini review. Electrochem. Commun. 2020, 115, 106722.
[33] Zhang, N.; Dong, Y.; Jia, M.; Bian, X.; Wang, Y.; Qiu, M.; Xu, J.; Liu, Y.; Jiao, L.; Cheng, F. Rechargeable aqueous Zn–V_2O_5 battery with high energy density and long cycle life. ACS Energy Lett. 2018, 3, 1366–1372.
[34] Zuo, S.; Xu, X.; Ji, S.; Wang, Z.; Liu, Z.; Liu, J. Cathodes for aqueous Zn-ion batteries: materials, mechanisms, and kinetics. Chem. Eur. J. 2021, 27, 830–860.
[35] Yang, G.; Wei, T.; Wang, C. Self-healing lamellar structure boosts highly stable zinc-storage property of bilayered vanadium oxides. ACS Appl. Mater. Interfaces. 2018, 10, 35079–35089.
[36] Hu, P.; Yan, M.; Zhu, T. Zn/V_2O_5 Aqueous Hybrid-Ion Battery with High Voltage Platform and Long Cycle Life. ACS Applied Materials & Interfaces. 2017, 9, 42717-42722.
[37] Yan, M.; He, P.; Chen, Y.; Wang, S.; Wei, Q.; Zhao, K.; Xu, X.; An, Q.; Shuang, Y.; Shao, Y.; Mueller, K. T.; Mai, L.; Liu, J.; Yang, J. *Adv. Mater.* 2018, 30, 1703725.
[38] Zhang, Y.; Ang, E.H.; Dinh, K.N.; Rui, K.; Lin, H.; Zhu, J.; Yan, Q. Recent advances in vanadium-based cathode materials for rechargeable zinc ion batteries. Mater. Chem. Front. 2021, 5, 744-762.
[39] Tamilselvan, M.; Sreekanth, T.V.; Yoo, K.; Kim, J. Self-doped 2D-V2O5 nanoflakes – A high electrochemical performance cathode in rechargeable zinc ion batteries. Ceramics International. 2021, 47, 29832-29839.
[40] Liu, C.; Neale, Z.G.; Zheng, J.; Jia, X.; Huang, J.; Yan, M.; Tian, M.; Wang, M.; Yang, J.; Cao, G. Expanded hydrated vanadate for high-performance aqueous zinc-ion batteries. Energy & Environmental Science. 2019, 12, 2273.
[41] Yuan, T.; Cheng, H.; Li, X.; Ren, H.; Hu, Y.; Chen, H.; Zhao, J.; Dai, S.; Liu, M.; Hu, H. Organic macromolecule regulated the structure of vanadium oxide with high capacity and stability for aqueous Zinc-ion batteries. Applied Surface Science. 2022, 592, 153295.
[42] Zuo, S.; Xu, X.; Ji, S.; Wang, Z.; Liu, Z.; Liu, J. Cathodes for Aqueous Zn-Ion Batteries: Materials, Mechanisms, and Kinetics. Chemistry: a European journal. 2021, 27, 830–860.
[43] Cui, H.; Ma, L.; Huang, Z.; Chen, Z.; Zhi, C. Organic materials-based cathode for zinc ion battery. SmartMat (Beijing, China). 2022, 3, 565–581.